OPTO-ELECTRONICS REVIEW **12**(4), 389–397

Anticipated performance characteristics of possible InP-based vertical-cavity surface-emitting diode lasers for the third-generation 1.55-μm optical fibre communication systems

S. MACEGONIUK, R.P. SARZAŁA, and W. NAKWASKI*

Laboratory of Computer Physics, Institute of Physics, Technical University of Łódź
219 Wólczańska Str., 93-005 Łódź, Poland

Anticipated performance of possible InP-based vertical-cavity surface-emitting lasers (VCSELs) for the third generation 1.55-μm optical-fibre communication has been simulated with the aid of the comprehensive optical-electrical-thermal-gain self-consistent model. While the room-temperature (RT) pulse operation of the above VCSELs has been found to be reached without serious difficulties, their efficient RT continuous-wave operation does not seem to be possible because of inherently insufficient physical properties of the $A^{III}P$ phosphides. Therefore, as the final conclusion of this paper, we have to stress that, taking into consideration currently available technology, InP-based VCSELs cannot be recommended as laser sources for future long-wavelength optical-fibre communication systems.

Keywords: InP-based VCSELs, 1.55-μm optical-fibre communication, simulation of a VCSEL operation.

1. Introduction

In commercial optical-fibre communication systems, gallium arsenide diode lasers are currently used to generate the 0.85-μm carrier wave. However, in the nearest future, these first-generation optical-fibre communication systems do not seem to be able to cope with dramatically increasing operational requirements associated with anticipated enormous demands of future Internet networks. Therefore the second-generation (based on the 1.3-μm carrier wave) and the third-generation (1.55 μm) optical-fibre communication systems are being worked out now. Unfortunately, relatively cheap and high-reliability standard GaAs-based diode lasers cannot be used in these new systems.

Currently, InP-based diode lasers are the only semiconductor lasers commercially available in this long-wavelength emission range. While their edge-emitting designs seem to meet general expectations, their vertical-cavity surface-emitting diode laser (VCSEL) configurations are still far from being optimal. It creates a serious problem, because just VCSELs are believed to be inherently the best suited diode-laser configuration for the optical fibre communication. The most severe difficulty to manufacture cheap and high-performance InP-based VCSELs is associated with their high-reflectivity resonator mirrors and efficient confining mechanisms of both a current spreading and an optical field.

In the present paper, an attempt to design appropriate 1.55-μm InP-based VCSELs is made. Their possible structures will be optimised and their operational characteristics will be anticipated with the aid of a modern computer experiment method. A comprehensive, fully self-consistent optical-electrical-thermal-gain model will be formulated to this end on the basis of principles given in Ref. 1.

2. Hitherto reported designs of 1.55-μm InP-based VCSELs

At the Royal Institute of Technology (KTH) in Stockholm, a mesa design of the InP-based VCSEL has been reported [2,3]. The laser has been equipped with the semiconductor (GaIn)(AsP)/InP distributed-Bragg-reflector (DBR) bottom mirror and the dielectric Si/SiO_2 DBR output (15-μm diameter) upper mirror. Because of low electrical conductivity of dielectric mirrors, annular p-side contact has been used. The 17-μm-diameter etched mesa has been surrounded by the polyamide layer. While the pulse operation of the laser has been achieved up to 45°C, its continuous-wave (CW) operation is possible only below –22°C. Because of nonradiative surface recombination, room-temperature (RT) pulse threshold current as high as 13 kA/cm^2 has been reported. Some improvements have been achieved after replacing the polyamide with the semi-insulating InP:Fe layer, but the RT CW operation has still remained for this laser unachievable.

Essential improvements have been reached in the next InP-based VCSEL reported by KTH [4]. This time the up-

*e-mail: nakwaski@p.lodz.pl

per dielectric DBR mirror from the previous design has been replaced with the semiconductor GaAs/(AlGa)As one fused to the main laser body. The above enables selective radial oxidation of AlAs-rich layers creating oxide apertures for current funnelling. Afterwards, the broad-area p-side contact has been created on the upper mirror and the output beam has been directed through the bottom DBR. Improving uniformity of current injection into an active region has enabled reduction of the RT pulse threshold-current density to only 1.8 kA/cm^2. Besides, the RT CW operation has been possible up to 17°C.

Next step in a InP-based VCSEL modification has been to fuse both GaAs-based DBR mirrors on both sides of the (GaIn)(AsP)/InP multi-quantum-well (MQW) active region, which has been reported by the University of California at Santa Barbara (UCSB) [5]. No current confinement has been applied. RT CW operation has been achieved in this laser up to 33°C. An addition of the oxide aperture and the superlattice barrier has enabled increasing this temperature to 71°C [6] and later even to 105°C [7].

Composite resonator mirrors, i.e., the dielectric SiO_2/TiO_2 DBR deposited on the (GaIn)(AsP)/InP DBR as the upper mirror and the AlAs/GaAs DBR waver-fused to the (GaIn)(AsP)/InP DBR as the output bottom mirror, have been applied in 1.55-μm VCSEL reported by Nippon Telephone and Telegraph Corporation (NTT) [8,9]. In these VCSELs, RT CW operation has been achieved up to 27°C and their threshold current densities have been equal to 1.8 kA/cm^2.

Even more advanced 1.55-μm completely monolithic VCSEL design has been reported by Alcatel [10]. In its manufacturing, expensive and very troublesome wafer-fusion technology has been avoided. Instead, metamorphic growth of arsenide DBR on phosphide structure has been used. Current confinement has been realized with the aid of proton implantation. Besides, a tunnel junction has been created which enables replacement of the p-type DBR mirrors with the n-type ones, leading to some essential reduction of the device series resistance and optical losses.

3. Selection of an appropriate 1.55-μm InP-based VCSEL structures

Local-area-networks (LANs) and metro-area-networks (MANs) of a steadily increasing density need many VCSEL lasers emitting the carrier wave. Both the above networks occupy more than 80% of the market [11]. Therefore a price of these lasers is of a special importance. It is easy to conclude from the above argumentation that very expensive and troublesome wafer-fusion technology cannot offer any solution to this problem. Besides, using this technology, mass production of diode lasers is practically impossible. What is more, wafer-fused devices do not seem to ensure sufficiently high reliability within the required [12,13] temperature range (from –40°C to 85°C) of telecommunication devices because of stresses generated at the InP/GaAs heterojunctions. Therefore, our model structure of VCSELs under consideration is based on the VCSEL design [2,3] reported by KTH.

The model VCSEL structure is schematically shown in Fig. 1. While its bottom 200-μm-diameter resonator mirror is assumed to be the 50-period quarter-wave n-type (GaIn)(AsP)/InP DBR doped with Si ($N_D = 5\times10^{18}$ cm^{-3}), the upper output 15-μm-diameter mirror is the analogous 5-period dielectric SiO_2/TiO_2 DBR. Theoretically determined mirror reflectivities are equal to 99.97% for the bottom mirror and to 99.62% for the upper output one. The resonator length is equal to 5 wavelengths of the laser radiation. The multi-quantum-well (MQW) active region [14] is composed of nine 7-nm $In_{0.774}Ga_{0.226}As_{0.78}P_{0.22}$ quantum wells (QWs) separated by 8.6-nm $In_{0.536}Ga_{0.464}As_{0.78}P_{0.22}$ barriers. The active region is confined by InP spacers: the 1.95-μm-thick p-side one and the 0.166-μm-thick n-side one. Radial optical confinement is accomplished by the upper 17-μm-diameter mesa structure of a thickness of 1.6 μm etched using the RIE method. An area around the mesa has been filled with the 1.6-μm-thick polyamide layer first, but much better results have been achieved with the semi-insulating InP:Fe of a much higher value of the thermal conductivity. The annular p-side contact of the 15-μm internal radius is deposited around the upper DBR mirror. To enhance the radial current flow from the p-side annular contact towards the centrally located active region, the p-type layer directly below the upper mirror is heavily doped ($N_D = 1\times10^{19}$ cm^{-3}). The VCSEL structure is manufactured on the n-type InP 0.45-μm-thick substrate which is attached to the 5-mm-thick copper heat sink.

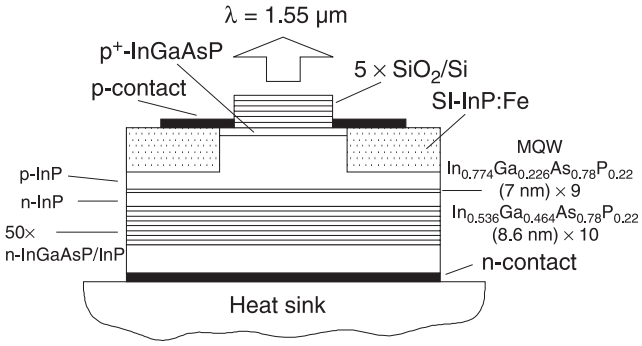

Fig. 1. The model InP-based VCSEL structure for the 1.55-μm optical-fibre communication systems.

4. The model

The comprehensive three-dimensional (3D) optical-electrical-gain-thermal self-consistent model of InP-based diode vertical-cavity surface-emitting lasers (VCSELs) has been developed to investigate their threshold room-temperature (RT) operation. Both pulse and continuous-wave (CW) RT operations are considered.

The computer model consists of four interrelated parts:

- the optical model describes, for successive radiation modes, optical fields within the resonator. The model is based on the effective frequency method [15]. The lasing threshold is determined from the condition of the real propagation constant.
- the finite-element (FE) electrical model characterizes both the current spreading (including carrier drift and diffusion processes) within the device volume between the top and the bottom contacts and the injection of both electrons and holes into the active region.
- the FE thermal model gives details of a heat generation (non-radiative recombination, reabsorption of radiation as well as the volume and the barrier Joule heating) and its spreading from the heat sources towards the heat sink.
- the gain model, based on the Fermi's Golden Rule, gives information about the optical gain spectra.

Besides, all important, usually non-linear, interactions between the above physical phenomena are taken into account using the self-consistent algorithm of calculations shown in Fig. 2. More details about the simulation model may be found in our previous publications, e.g, in Refs. 16, 17, and 18.

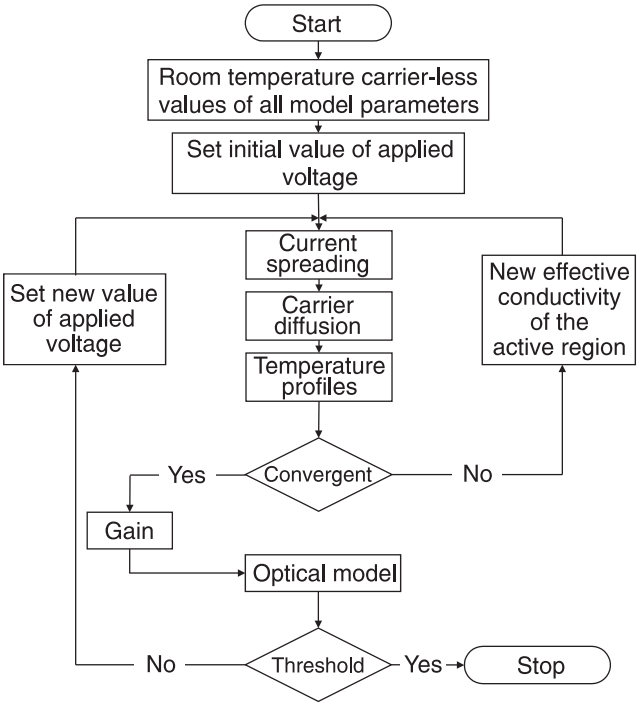

Fig. 2. Flow chart of the self-consistent model calculations.

5. Numerical data

5.1. Material parameters used in the electrical model

Room-temperature values of electrical conductivities used in our model are equal to 6.4×10^3 $(\Omega\,\mathrm{m})^{-1}$ for the p-type (GaIn)(AsP) layer [19,20], to 1.12×10^3 $(\Omega\,\mathrm{m})^{-1}$ for the p-type InP layer [19,20], to 3.68×10^5 $(\Omega\,\mathrm{m})^{-1}$ for the n-type (GaIn)(AsP) layer [19,20] and the n-type InP layer [5,20,21], to 2.7×10^{-8} $(\Omega\,\mathrm{m})^{-1}$ for the semi-insulating InP:Fe layer [4], to 5.88×10^7 $(\Omega\,\mathrm{m})^{-1}$ for the copper layer, and to 5 $(\Omega\,\mathrm{m})^{-1}$ for the p-side contact. Temperature dependences of electrical conductivities are in considered semiconductors mostly connected with changes of carrier mobilities. For the considered temperature range between 300 K and 400 K, they are assumed on the basis of results reported in [19,20] to be proportional to $T^{-1.25}$ (for n-type InP and n-type (GaIn)(AsP)], to T^{-2} (for *p*-type InP) or to $T^{-2.2}$ [for p-type (GaIn)(AsP)].

The following temperature dependences of the recombination coefficients, namely the monomolecular A coefficient [22,23], the bimolecular B coefficient [20,22,24–26] and the Auger C coefficient [20,24], are assumed on the basis of reported experimental data

$$A(T) = 1.1\times10^8\ \mathrm{s}^{-1} \tag{1}$$

$$B(T) = [1\times10^{-10} - 2\times10^{-13}(T - 300\ \mathrm{K})]\ \mathrm{cm}^3/\mathrm{s} \tag{2}$$

$$C(T) = [7.5\times10^{-29} + 1.1\times10^{-31}\ (T - 300\ \mathrm{K})]\ \mathrm{cm}^6/\mathrm{s} \tag{3}$$

Analogously, the ambipolar diffusion coefficient is taken as [25]

$$D(T) = 5(T/300\ \mathrm{K})\ \mathrm{cm}^2/\mathrm{s} \tag{4}$$

5.2. Material parameters used in the thermal model

For semiconductor layers, temperature changes of the thermal conductivities k are assumed to be expressed by the following relations [19,27]

$$k(T) = \frac{100}{1.47 + \dfrac{T - 300}{111}}\ \mathrm{W/mK},\quad \text{for InP layers} \tag{5}$$

$$k(T) = 43\left(\frac{300}{T}\right)^{1.375}\ \mathrm{W/mK},\quad \text{for (GaIn)(AsP) layers} \tag{6}$$

Analogously, thermal conductivities are taken to be equal to 2.6 W/mK [28] for the Si layers, to 1.4 W/mK [28] for the SiO_2 layers, and to 398 W/mK [29] for the copper one.

5.3. Material parameters used in the gain model

Numerical data describing the active region under consideration calculated on the basis of formulae given by Li [30] or taken from [31] are listed in Table 1. Temperature variations of energy gaps are determined from the following Varshni formula

$$E_G(T) = E_G(0\mathrm{K}) - \frac{4.9\times10^{-4}\,T}{327 + T}\mathrm{eV}. \tag{7}$$

Table 1. Parameters used to determine gain spectra in the $In_{0.774}Ga_{0.226}As_{0.78}P_{0.22}/In_{0.536}Ga_{0.464}As_{0.78}P_{0.22}$ quantum well.

Parameter	Value
QW depth in the conduction band	108.4 meV
QW depth in the valence band	162.6 meV
Barrier depth in the conduction band	123.2 meV
Barrier depth in the valence band	228.8 meV
Spin-orbit splitting	316 meV
QW electron mass	0.045 m_0
QW heavy-hole mass	0.523 m_0
QW light-hole mass	0.058 m_0
Barrier electron mass	0.057 m_0
Barrier heavy-hole mass	0.518 m_0
Barrier light-hole mass	0.072 m_0
Matrix element	9.3 m_0 eV

5.4. Material parameters used in the optical model

Values of material parameters used in our optical model are listed in Table 2, where n_R and n_g stand for the phase and the group, respectively, refractive indices and α is the absorption coefficient. In InP-based lasers, the main absorption mechanism is associated with the intervalence band absorption. For λ = 1.55 μm and the active region under consideration, its temperature dependence may be expressed as [5]

$$\alpha_{MQW}(T) = 1.57 \times 10^{10} \exp\left(-\frac{0.5\text{eV}}{k_B T}\right)\text{cm}^{-1}, \qquad (8)$$

where k_B is the Boltzmann constant.

5.5. Diode parameters used in the electrical model

The diode current density/voltage equation may be expressed as

$$j = j_s[\exp(\beta_{pn} U_{pn}) - 1] \approx j_s \exp(\beta_{pn} U_{pn}), \qquad (9)$$

where j_s stands for the reverse saturation current density, U_{pn} is the p-n junction voltage drop and β_{pn} is the p-n junction parameter. On basis of experimental results reported in Refs. 2 and 3, the following RT values of the above parameters are determined: j_s = 1.0 A/m^2, β_{pn} = 23.0 V^{-1}.

6. Results

6.1. Verification of some designing assumptions

In our calculations, a perfect 100% efficiency of carrier injection into QWs has been assumed. To verify this assumption, the band structure (shown in Fig. 3 together with its surrounding) of the 1.55-μm multi-quantum-well (MQW) $In_{0.774}Ga_{0.226}As_{0.78}P_{0.22}$-$In_{0.536}Ga_{0.464}As_{0.78}P_{0.22}$ active region under consideration has been determined using data listed in Table 1. As one can see, carrier leakage is possible only for conduction-band electrons, but even in this case, because of the relatively high conduction-band potential step between the active region and the InP spacers, this leakage may be practically neglected, at least for the RT pulse VCSEL operation.

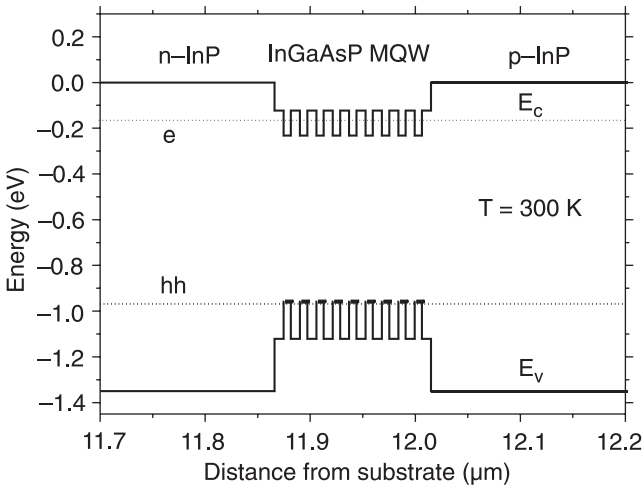

Fig. 3. Band structure of the unpolarized 1.55-μm multi-quantum-well (MQW) $In_{0.774}Ga_{0.226}As_{0.78}P_{0.22}$-$In_{0.536}Ga_{0.464}As_{0.78}P_{0.22}$ active region under consideration at RT. The lowest electron (*e*) and heavy-hole (*hh*) energy levels are shown as dotted lines. E_C and E_V are the edges of the conduction band and the valence band, respectively.

The laser has been designed for the 1.55-μm optical communication. Figure 4 presents gain spectra of the selected $In_{0.774}Ga_{0.226}As_{0.78}P_{0.22}$-$In_{0.536}Ga_{0.464}As_{0.78}P_{0.22}$ QW (supplied with carriers of the concentration of 4×10^{18} cm^{-3}) at and slightly above RT. It is seen from the above plots,

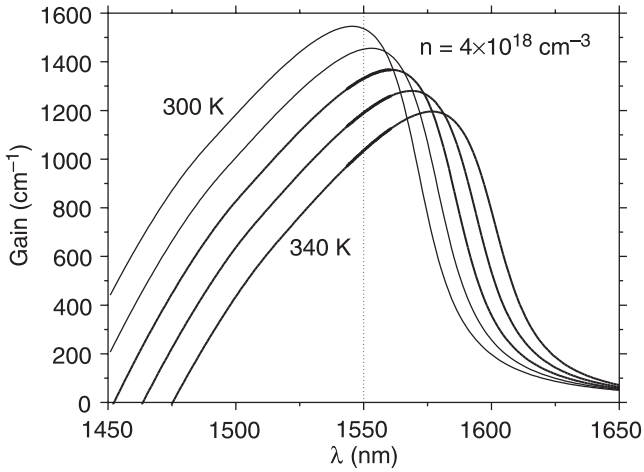

Fig. 4. Optical gain spectra at ambient temperatures changing by 10 K from RT for the QW under consideration ($In_{0.774}Ga_{0.226}As_{0.78}P_{0.22}$/$In_{0.536}Ga_{0.464}As_{0.78}P_{0.22}$ QW) supplied with the carrier concentration of 4×10^{18} cm^{-3}.

Table 2. Values of optical parameters.

Layer	n_R	n_g	Ref.	dn_R/dT (10^{-4}/K)	Ref.	α (cm^{-1})	Ref.
Si	3.61	3.816	[3,28]	1	[3]	400	[3]
SiO_2	1.45	1.491	[3,28]	0.1	[3]	0	[3]
p-(GaIn)(AsP)	3.46	3.46	[3]	2	[3]	240	[3]
p-InP	3.170	3.172	[3,5]	2	[3]	24	[3,5,32]
QW	3.6	3.6	[5]	2	[3]	54	[3]
Barrier	3.4	3.4	[5]	2	[3]	54	[3]
n-InP	3.170	3.172	[3,33]	2	[3]	8	[3,5]
n-(GaIn)(AsP)	3.46	3.46	[3]	2	[3]	8	[3]

that the QW composition has been chosen correctly for RT but any increase in the active-region temperature is followed by an undesirable red shift of the whole gain spectrum. Therefore, for the continuous-wave (CW) VCSEL operation, QW composition should be intentionally blue shifted at RT to ensure 1.55-μm laser emission at an increased active-region temperature.

The axial intensity profile (radiation standing wave) of the laser radiation within the 5λ VCSEL resonator is shown in Fig. 5 together with the refractive-index profile. Relatively small refractive-index contrast of the semiconductor DBR mirror compels us to apply as many as 50 DBR periods to ensure high enough mirror reflectivity. Nevertheless, a considerable penetration of the bottom semiconductor n-type DBR mirror by a radiation field is seen. Therefore possible loss mechanisms within these layers should be carefully controlled. From among them, the free-carrier absorption (about 8 cm^{-1}) is kept below the acceptable limit, but scattering and diffraction losses, associated for example with radiation scattering by not perfectly flat and parallel to one another edges of mirror layers, may become quite harmful, so the resonator mirrors need a very careful technology. The MQW active region is located exactly at the anti-node position of the radiation standing wave to increase an influence of an optical gain on laser intensity, i.e., to enhance coupling between the recombining carriers and the radiation field.

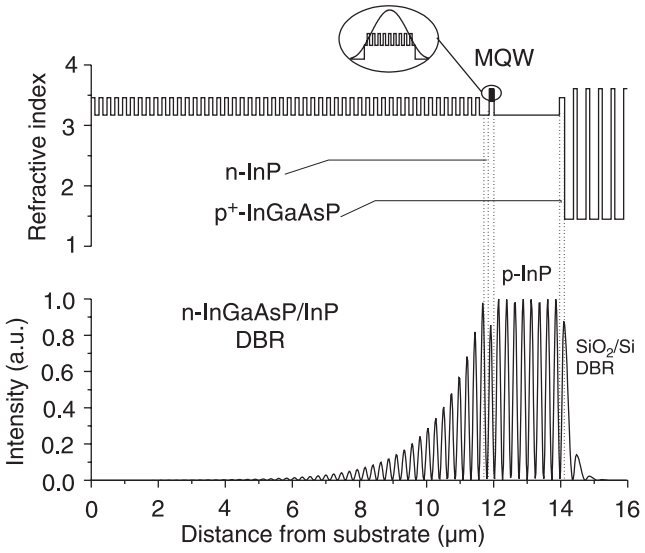

Fig. 5. The axial intensity profile (radiation standing wave) of the laser radiation within the 5λ resonator of the VCSEL under consideration during the laser RT pulse threshold operation.

6.2. RT pulse operation

An estimated RT pulse threshold current of the InP-based VCSEL under consideration is equal to about 15 mA, which corresponds to the supplied voltage of about 1.3 V. For these operation conditions, two-dimensional (2D) plots of the potential distribution within the laser structure is shown in Fig. 6. As one can see, potential is changing rapidly below the p-side annular contact. From these spatial potential profiles, a very intense radial current flow towards the laser axis through the thin but highly-doped p$^+$-(GaIn)(AsP) layer and the p-type InP spacer may be deduced. As a result, the radial profile of a current-density j_{pn} injected into the active region (Fig. 7) is quite well confined within the 15-μm-diameter active region. However, some undesirable current penetration of lateral $r > 7.5$ μm lossy areas is also observed. Nonuniformity of a current injection is followed by an analogous (although considerably less intense) nonuniformity of the radial active-region carrier-concentration profile (Fig. 8) leading to a similarly nonuniform radial distribution of an optical gain. This may favour higher-order transverse modes (instead of a desired fundamental LP_{01} one) and needs some additional designing solution. The potential changes along the VCSEL axis is plotted in Fig. 9 for the laser RT pulse threshold operation. As one can see, the p-n junction voltage drop is equal to about 0.8 V, which corresponds to the desired wavelength of an emitted radiation of 1.55 μm.

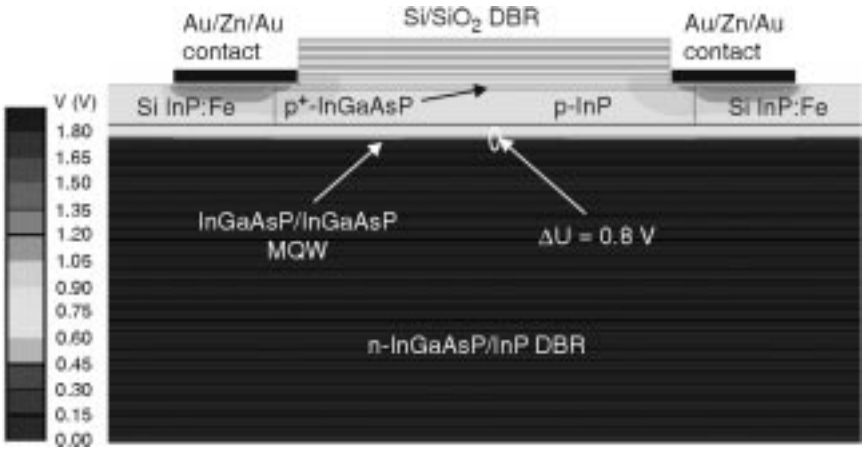

Fig. 6. 2D potential profiles within the considered structure of InP-based VCSEL for its RT pulse threshold operation (U = 1.3 V, I = 15 mA).

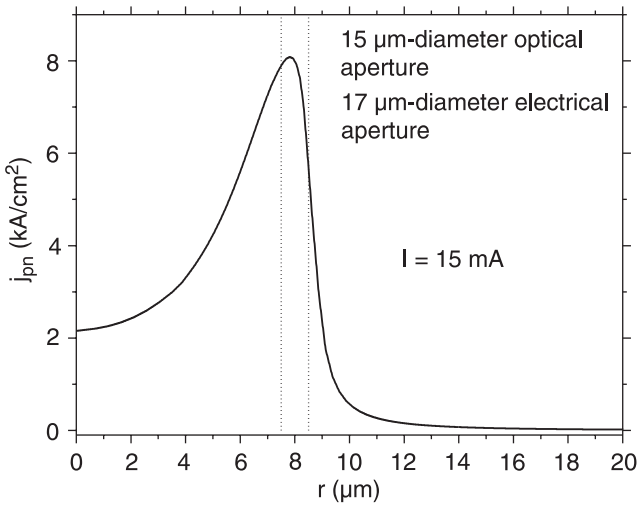

Fig. 7. Radial profile of the current-density j_{pn} injected into the active region for the RT threshold pulse VCSEL operation.

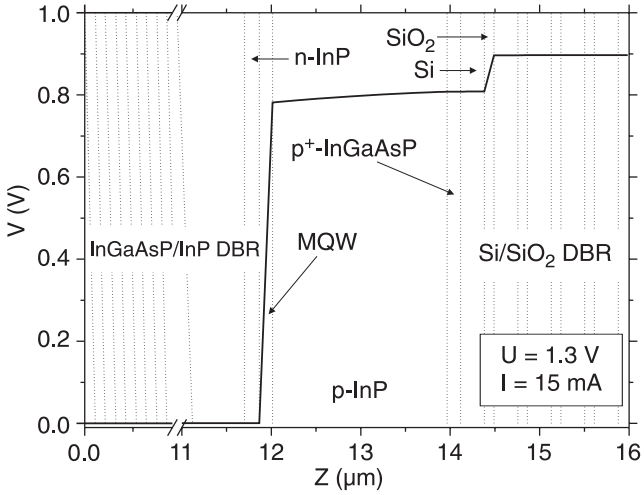

Fig. 9. Potential changes along the laser axis of the VCSEL under consideration for its RT threshold pulse operation.

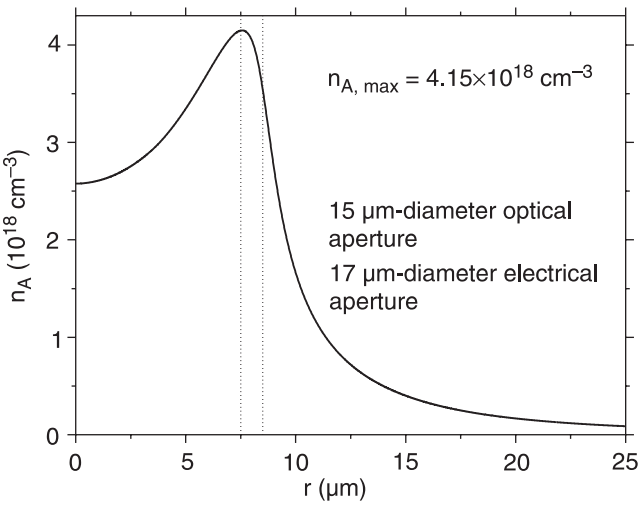

Fig. 8. Radial profile of the active-region carrier concentration n_A for the RT threshold pulse VCSEL operation.

6.3. An attempt to reach the RT CW operation

The tentative continuous-wave RT operation of the InP-based 1.55-μm VCSEL is considered in next figures. For these operation conditions, both the p-n junction current density profiles (Fig. 10) and the active-region carrier concentration profiles (Fig. 11) exhibit a considerable penetration of the lateral ($r > 7.5$ μm) lossy areas to much more extent than previously for the RT pulse operation. Besides, the above profiles within the active region are also much more nonuniform which makes even more difficult the tentative RT CW fundamental LP_{01} mode operation. Fortunately, active-region temperature distributions (Fig. 12) may, at least partly, compensate the above gain-related antiguiding effect with the thermal focusing one. But these temperature increases, as high as nearly 85 K for the supply voltage of 2.5 V, are also followed by some unprofitable consequences: the gain peak is considerably reduced and red shifted (c.f. Fig. 4) as well as optical absorption and loss mechanisms are enhanced. The last effect is illustrated

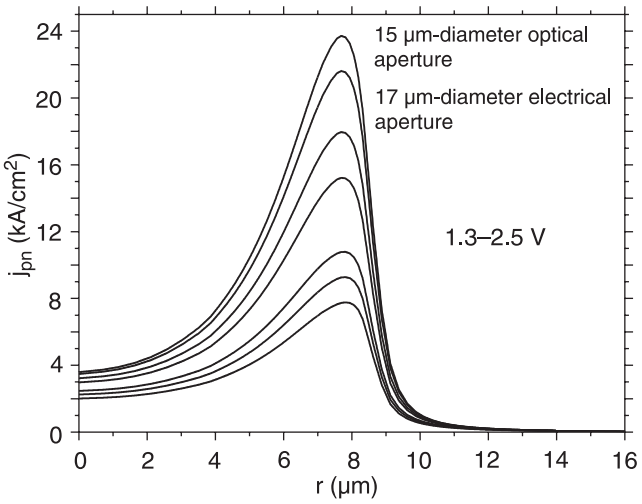

Fig. 10. Radial profiles of the p-n junction current density $j_{pn}(r)$ for various values of a supply voltage of the tentative RT CW operated VCSEL.

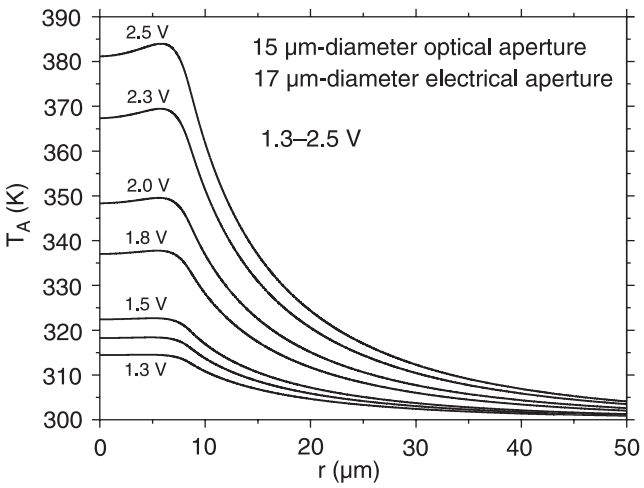

Fig. 12. Radial profiles of the active-region temperature T_A for various values of a supply voltage of the tentative RT CW operated VCSEL.

in Fig. 13. As expected, the non-radiative Auger recombination is in the InP-based VCSEL under consideration a dominant recombination mechanism, especially for a higher operation voltage, which means, for higher active-region temperature increases [c.f. Eq. (3)]. Besides, optical absorption [mostly of inter-valence type (in the p-type phosphides) associated with electron transitions between the spin-orbit split band and the heavy-hole band] depends exponentially on temperature [c.f. Eq. (8)].

All the above effects stimulated by temperature increases, i.e., more non-uniform optical gain profiles within the VCSEL active region, a reduced peak value of an optical gain and its red shifting, an increase in both the nonradiative shares of an operation current and the optical absorption coefficients, make difficult reaching the RT CW lasing thresholds of the InP-based 1.55-μm diode VCSELs.

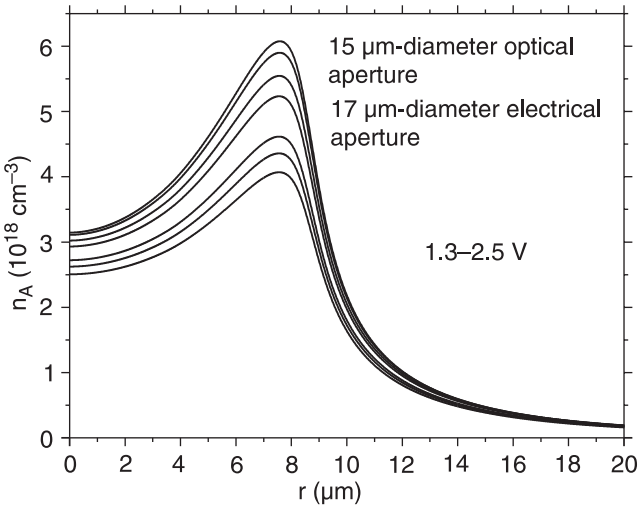

Fig. 11. Radial profiles of the p-n active-region carrier concentration $n_A(r)$ for various values of a supply voltage of the tentative RT CW operated VCSEL.

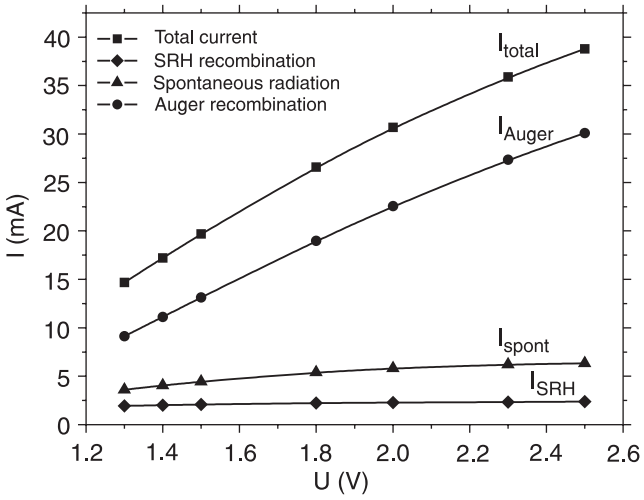

Fig. 13. The total operation current I_{total} and its constituent parts associated with the Auger recombination (I_{Auger}), with the bimolecular radiative recombination (I_{spon}) and with the Shockley-Read-Hall monomolecular non-radiative recombination (I_{SRH}) versus the supply voltage U of the tentative RT CW operated VCSEL.

In fact, within a validation range of our simulation model, we could not reach the RT CW operation of the VCSEL under consideration at all.

7. Conclusions

The main goal of this work, which means an attempt to design the InP-based 1.55-μm diode VCSEL for its efficient and reliable RT CW operation, has not been achieved. Although the RT pulse threshold operation of the above laser seems to be reached without serious difficulties, its RT CW lasing operation turns out to be unattainable. It is a consequence of inherently insufficient physical properties of the

$A^{III}P$ phosphides and their strong temperature sensitivity. In particular:

- because of a low contrast between refractive indices of InP and (GaIn)(AsP) layers, very many periods of phosphide DBR mirrors are necessary to reach required mirror reflectivities. Besides, their electrical resistivities are very high, which increases the Joule heating. Unfortunately, these resistivities cannot be reduced by increasing doping because of rising optical absorption. What is more, thermal conductivities of quaternary (GaIn)(AsP) layers are extremely low, which impedes heat-flux abstraction process towards the laser heat-sink. All the above phenomena are followed by a considerable temperature increase within semiconductor phosphide DBRs.
- the non-radiative Auger recombination is in the $A^{III}P$ phosphides at RT a dominant recombination mechanism, especially for higher operation currents, competing with the binary radiative recombination. Besides, as a result of the Auger recombination, an additional active-region temperature increase is observed which additionally enhances the strongly temperature-dependent Auger recombination.
- for the RT CW operation, conduction-band quantum wells may become too low to effectively suppress an electron leakage.

The above unprofitable effects are very difficult to be avoided because they are inevitable consequences of inherent phosphide physical properties. Some attempts, mostly with the aid of the waver-fusion technology, have been reported and an efficient RT CW operation of InP-based VCSELs has been reported (see Sect. 2). However, for the mass optical-fibre communication systems, their reliability seems to be insufficient, their price – much too high, and their production – too troublesome. So our final conclusion is not beneficial for InP-based 1.55-μm VCSELs – they are not suitable laser sources for the future high-performance long-wavelength optical-fibre communication systems.

Acknowledgements

This work was supported by the Polish State Committee for Scientific Research (KBN), grants nos. 7-T11B-073-21 and 4-T11B-014-25.

References

1. M. Osiński and W. Nakwaski, "Three-dimensional simulation of vertical-cavity surface-emitting semiconductor lasers", in *Vertical-Cavity Surface-Emitting Laser Diodes*, Chapter 5, pp. 135-192, edited by Li and K. Iga, Springer, Berlin, 2003.
2. K. Streubel, S. Rapp, J. Andre, and J. Wallin, "Room-temperature pulsed operation of 1.5-μm vertical cavity lasers with an InP-based Bragg reflector", *IEEE Photon. Techn. Lett.* **8**, 1121–1123 (1996).
3. S. Rapp, J. Piprek, K. Streubel, J. Andre, and J. Wallin, "Temperature sensitivity of 1.54 μm vertical-cavity lasers with an InP-based Bragg reflector", *IEEE J. Quantum Electron.* **33**, 1839–1845 (1997).
4. S. Rapp, "Long-wavelength vertical-cavity lasers based on InP/GaInAsP Bragg reflectors", *Doctoral Thesis*, KTH Stockholm, 1999.
5. J. Piprek, D.I. Babić, and J.E. Bowers, "Simulation and analysis of 1550 nm double-fused vertical-cavity lasers", *J. Appl. Phys.* **81**, 3382–3390 (1997).
6. K.A. Black, P. Abraham, N.M. Margalit, E.R. Hegblom, Y.-J. Chiu, J. Piprek, J.E. Bowers, and E.L. Hu, "Double-fused 1.5 μm vertical-cavity lasers with record high T_0 of 132 K at room temperature", *Electron. Lett.* **34**, 1947–1949 (1998).
7. A. Karim, P. Abraham, D. Lofgreen, Y.-J. Chiu, J. Piprek, and J.E. Bowers, "Waferbonded 1.55 μm vertical-cavity lasers with continuous-wave operation up to 105°C", *Appl. Phys. Lett.* **78**, 2632–2633 (2001).
8. Y. Ohiso, H. Okamoto, Y. Itoh, K. Tateno, T. Tadokoro, H. Takenouchi, and T. Kurokawa, "1.55-μm vertical-cavity surface-emitting lasers with wafer-fused GaInAsP/InP-GaAs/AlAs DBRs", *Electron. Lett.* **32**, 1483–1484 (1996).
9. Y. Ohiso, C. Amano, Y. Itoh, H. Takenouchi, and T. Kurokawa, "Long-wavelength (1.55-μm) vertical-cavity lasers with InGaAsP/InP – GaAs/AlAs DBR's by wafer fusion", *IEEE J. Quantum Electron.* **34**, 1904–1913 (1998).
10. L. Goldstein, C. Fortin, C. Starck, A. Plais, J. Jacquet, J. Boucart, A. Rocher and C. Poussou, "GaAlAs/GaAs metamorphic Bragg mirror for long-wavelength VCSEL's", *Electron. Lett.* **34**, 268–270 (1998).
11. J. McEntee, "…while global optical-fibre market flatlines", *Fibre Systems* **1**, 7 (2004).
12. W. Ha, V. Gambin, M. Wistey, S. Bank, S. Kim, and J.S. Harris Jr., "Multiple-quantum-well GaInNAs-GaNAs ridge-waveguide laser diodes operating out to 1.4 μm", *IEEE Photonics Technology Letters* **14**, 591–593 (2002).
13. S. Bank, W. Ha, V. Gambin, M. Wistey, H. Yuen, L. Goddard, S. Kim, and J.S. Harris Jr., "1.5-μm GaInNAs(Sb) lasers grown on GaAs by MBE", *J. Cryst. Growth* **251**, 367–371 (2003).
14. K. Streubel, J. Wallin, G. Landgren, U. Ohlander, S.Lourdudoss, and K. Kjebon, "Importance of metalorganic vapour phase epitaxy growth conditions for the fabrication of GaInAsP strained quantum well lasers", *J. Cryst. Growth* **143**, 7–14 (1994).
15. H. Wenzel and H.-J. Wünsche, "The effective frequency method in the analysis of vertical-cavity surface-emitting lasers", *IEEE J. Quantum Electron.* **33**, 1156–1162 (1997).
16. P. Maćkowiak and W. Nakwaski, "Designing guidelines for possible continuous-wave-operating nitride vertical-cavity surface-emitting lasers", *J. Phys. D: Appl. Phys.* **33**, 642–653 (2000).
17. W. Nakwaski, "Simulation of optical phenomena in vertical-cavity surface-emitting lasers: I. Fundamental principles", *Opto-Electron. Rev.* **8**, 83–90 (2000).
18. R.P. Sarzała, P. Mendla, M. Wasiak, P. Mackowiak, M. Bugajski, and W. Nakwaski, "Comprehensive self-consistent three-dimensional simulation of an operation of the GaAs-based oxide-confined 1.3-μm quantum-dot (InGa)As/GaAs vertical-cavity surface-emitting lasers", *Opt. Quantum Electron.* **37**, (2004). (in print)

19. S. Adachi, *Physical Properties of III-V Semiconductor Compounds*, Wiley, New York 1992.
20. http://www.ioffe.rssi.ru/SVA/NSM/Semicond
21. J. Piprek, "Electro-thermal analysis of oxide-confined vertical-cavity lasers", *Phys. Stat. Sol. (a)* **188**, 905–912 (2001).
22. J. Minch, S.H. Park, T. Keating, and S.L. Chuang, "Theory and experiment of InGaAsP and InGaAlAs long wavelength strained quantum-well lasers", *IEEE J. Quantum Electron.* **35**, 771–782 (1999).
23. A.P. Mozer, S. Hausser, and M.H. Pilkuhn, "Quantitative evaluation of gain and losses in quaternary lasers", *IEEE J. Quantum Electron.* **QE-21**, 719–725 (1985).
24. G.P. Agrawal and N.K. Dutta, *Long-Wavelength Semiconductor Lasers*, Van Nostrand Reinhold Company, New York, 1986.
25. O. Gilard, "Theoretical study of radiation effects on GaAs/AlGaAs and InGaAsP/InP quantum-well lasers", *J. Appl. Phys.* **93**, 1772–1780 (2003).
26. J.M. Pikal, C.S. Menoni, and H. Temkin, "Carrier lifetime and recombination in long-wavelength quantum-well lasers", *IEEE J. Select. Topics Quantum Electron.* **5**, 613–619 (1999).
27. W. Nakwaski, "Thermal conductivity of binary, ternary, and quaternary III–V compounds", *J. Appl. Phys.* **64**, 159–166 (1988).
28. A. Karim, S. Bjorlin, J. Piprek, and J. Bowers, "Long-wavelength vertical-cavity lasers and amplifiers", *IEEE J. Select. Topics Quantum Electron.* **6**, 1244–1253 (2000).
29. P. Maćkowiak, "Development of a structure of nitride vertical-cavity surface-emitting laser, its optimisation using self-consistent three-dimensional model of operation", *PhD Thesis Dissertation*, Institute of Physics, Technical University of Łódź, 2002. (in Polish)
30. E.H. Li, "Material parameters for InGaAsP and InAlGaAs systems for use in quantum-wells structures at low and room temperatures", *Physica* **E5**, 215–273 (2000).
31. S. Kakimoto and H. Watanabe, "Intervalence band absorption loss coefficients of the active layer for InP based long wavelength laser diodes", *J. Appl. Phys.* **87**, 2095–2097 (2000).
32. J. Taylor and V. Tolstikhin, "Intervalence band absorption in InP and related materials for optoelectronic device modeling", *J. Appl. Phys.* **87**, 1054–1059 (2000).
33. B. Sermage, H.J. Eichler, J.P. Heritage, R.J. Nelson, and N.K. Dutta, "Photoexcited carrier lifetime and Auger recombination in 1.3-μm InGaAsP", *Appl. Phys. Lett.* **42**, 259–261 (1983).

New laser diode modules with TTL modulation

Photonic Products Ltd has added TTL modulation options to it's Photon Module range of laser diode modules. The TTL modulation input will accept signals from DC up to 100 kHz minimum.

Modulation options are available on all Photon PM and Photon Plus PPM laser modules with wavelengths from 635nm-830nm and output powers from 0.9 mW to 32 mW. Customer-adjustable lens for collimated or focused beam may be replaced by other optical systems such as line generators. Operating voltage is from 2.7 V to 6 V for CW modules and 4–12 V for modules with TTL modulation.

The laser modules are designed for use where detection of the laser beam in high ambient light conditions is vital, such as security systems and safety barriers. Other applications include industrial alignment and positioning.

The modules consist of an anodised aluminium housing, laser diode, drive circuit and collimating lens, either cylindrical or with a 25 mm mounting flange. Mechanical dimensions are 12 mm diameter, 43 mm length and all standard Photon Module options are available. They can be supplied in various colours to assist in wavelength or power identification. Electrical connections are made via external flying leads.

Photonic Products is a manufacturer of innovative optoelectronic components based on semiconductor diode laser technology, offering product design from concept to production. We are also a specialist distributor of high performance industrial diode lasers for Sanyo, Sony & Opnextends

Data sheets are available to download from the Photonic Products website, http://www.photonic-products.com/productlist.htm

This news release is issued in accordance with clause 1.2j of the British Codes of Advertising and Sales Promotion, and therefore cannot be subject to a transaction of any kind.

Wendy Seegar
Photonic Products Ltd
E-mail: wendy.seegar@photonic-products.com
Tel: +44 (0)1279 719190
Fax: +44 (0)1279 719191
http://www.photonic-products.com

